Materials
Views
www.MaterialsViews.com

ADVANCED MATERIALS
www.advmat.de

COMMUNICATION

Macroscopic Single-Crystal Gold Microflakes and Their Devices

Jiyu Zhou, Abhijit Saha, Jozef Adamcik, Haiqing Hu, Qingshan Kong, Chaoxu Li,* and Raffaele Mezzenga*

Nature offers countless examples of systems with remarkable 2D physical properties, e.g., anisotropic conductivity of graphite,[1] optical properties of nacre,[2] and superstrong mechanical property of bones.[3] These intriguing shape/size-dependent properties have inspired the synthesis of a wide variety of 2D-layered nanomaterials.[4] In particular, the quantum 2D confinement of electrons found in graphene nanosheets implies that 2D metal nanomaterials may bear unique catalytic, electrical, magnetic, and optical properties controlled by their geometric feature.[5] For example, gold platelets/nanosheets have size-dependent surface plasmon absorption in the visible-near-infrared region, and their sharp edges and corners can act as nanofocus sources to improve fluorescence, Raman scattering, single-molecule detection and nonlinear nanospectroscopy.[6] Their large aspect ratio can assist in the top–down fabrication of optical nanocircuitry for high-speed communication,[7] as well as in the organization into layered composites for specific functions.[8,9] The atomically flat surfaces of single-crystal gold 2D nanomaterials provide an ideal platform for single-molecule sensing and imaging.[7] However, it remains highly challenging to transfer this 2D effect to macroscopic length scales serving technological applications in catalysis, sensing, optoelectronic devices and conductive composites.

In the past decades, much endeavor has been devoted to develop shape/size-controlled bottom-up approaches to synthesize gold 2D nanomaterials with high yield. Micro- or sub-micrometric single-crystal gold platelets were frequently prepared by reducing chloroaurate ions with wet chemical, electrochemical, photochemical, and thermal reduction methods in the presence of soft templates, capping agents or interfaces.[10–15] Single-crystal gold nanosheets with the planar area up to 10^2 μm^2 were also synthesized from chloroaurate ions by several research groups, such as by Jiu et al. in the presence of ethylene glycol and polyvinylpyrolidone,[16] by Qin et al. in the presence of dodecyl glyceryl itaconate,[17] and by Li et al. in the presence of ionic liquid.[18] Recent efforts have converged on environmental friendly and low cost synthesis routes, particularly exploiting the use of biomolecules and biopolymers, e.g., chitosan,[19] arginine,[9] combination of H_2O_2 and starch,[10] and amyloid fibrils.[8] In all the above cases, chloroaurate ions were reduced in a controllable way, and gold single crystals underwent a nucleation and 2D growth process from sub-nanometric to micrometric lateral length scales. Yet, and despite several examples of macroscopic crystals found in nature, to the best of our knowledge, these synthesis approaches have not been successful to extend the single-crystal gold nanosheets to macroscopic scales, or, in other words, to a length scale accessible to the human eye resolution regime, i.e., with planar area $\geq 10^3$ μm^2 (microflakes). The only macroscopic gold microflakes reported to date are gold foils engineered from nugget in top-down approaches, e.g., via vapor deposition and hammering, which, however, are incredibly energy-consuming, polycrystalline and with rough surfaces.[20–22] Thus, a simple, green and efficient method to prepare macroscopic single-crystal gold microflakes remains challenging, yet highly desirable in synthetic chemistry, material science, and nanotechnology.

In sharp contrast to the previous techniques of directionally growing 2D gold crystals using templates and interfaces,[17,23,24] it was recently found that certain biomaterials or their assemblies alone could act as both reducing agent and capping agent to prepare 10^2 μm^2 single-crystal gold nanosheets.[8,9] Herein, we show that by carefully tuning the concentrations of chloroaurate ions and amyloid fibrils as well as their ratio, single-crystal gold microflakes with an unprecedented planar area over 10^4 μm^2 and thickness larger than 100 nm can be prepared in a simple and highly scalable one-step green synthesis process. Despite being two orders of magnitude larger than the 2D gold single crystals previously reported in literature, they remain single-crystalline with regular shapes and atomically flat surfaces. Production of large gold microplates with thickness exceeding 100 nm has immediate relevance in a number of fields. For example, edge sizes exceeding 100 nm allow edible and cosmetic applications without the compulsory declaration of use of nanoparticles in the formulation, in agreement with European regulations (ISO/TS 27687:2008). Moreover, we demonstrate that these new materials enable producing flexible and electrically conductive composite films with strain/force-sensing properties in a facile, one-step casting method.

The synthesis of single-crystal gold microflakes was carried out at 60 °C and pH 2 in aqueous solutions containing predetermined concentrations of hydrogen tetrachloroaurate and β-lactoglobulin amyloid fibrils. Amyloid fibrils are

J. Zhou, Prof. Q. Kong, Prof. C. Li
Qingdao Institute of Bioenergy and Bioprocess Technology
Chinese Academy of Sciences
Songling Road 189, Qingdao 266101, P.R. China
E-mail: licx@qibebt.ac.cn
J. Zhou, Prof. H. Hu
Department of Polymer Science and Engineering
Qingdao University of Science and Technology
Zhengzhou Road 53, Qingdao 266042, P.R. China
Dr. A. Saha, Dr. J. Adamcik, Prof. R. Mezzenga
ETH Zurich, Food and Soft Materials
Department of Health Science & Technology
Schmelzbergstrasse 9, LFO, E23 8092, Zürich, Switzerland
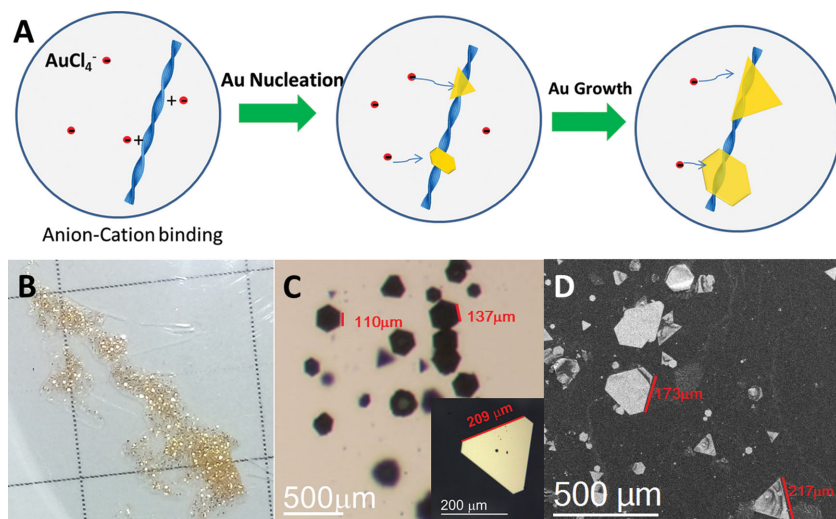E-mail: raffaele.mezzenga@hest.ethz.ch

Figure 1. A) Schematic synthesis procedure of macroscopic single-crystal gold microflakes from chloroaurate ions and amyloid fibrils, and their images by B) visual observation (grid size 0.9 × 0.9 cm²); C) optical microscopy; and D) SEM.

experimental conditions, single-crystal gold microflakes can be obtained with their lateral edge size over 0.1 mm. In this study, we classify the 2D gold materials into three categories according to their planar area: platelets (<1 μm²), nanosheets (1–10³ μm²), and microflakes (>10³ μm²) (Figure S1, Supporting Information).

Figure 1B–D shows representative images of the resulting 2D gold materials with microflakes, where amyloid fibrils are invisible due to their nanoscale diameter (Figure S2, Supporting Information). Due to their large planar area over 10⁴ μm² and atomically flat surfaces, individual gold microflakes can be easily distinguished by naked eyes in Figure 1B. Brightness, darkness, and golden color arise due to different reflecting angles of microflakes to the camera lens. Further observations via optical microscopy (OM) and scanning electron microscopy (SEM) in Figure 1C,D, reveal hexagonal and triangular geometries in a symmetry characteristic of their (111) Fm3m plane and single crystalline features.[8,25] With the coexistence of platelets and nanosheets, a few microflakes have the lateral dimension up to 217 μm in the case of triangle, and 137 μm in the case of hexagon, corresponding to the planar area of 2.0×10^4 and 4.9×10^4 μm², respectively. The lateral edge size is one order of magnitude larger than that of single-crystal gold nanosheets we synthesized before; whereas, the planar area is two order of magnitude larger (for a comparison of the triangular geometry see Figure S3, Supporting Information).[8]

The synthesis conditions of microflakes were optimized by varying concentrations of chloroaurate ions and amyloid fibrils under constant pH ≈ 2 and temperature ≈60 °C. As shown in **Figure 2**, by adding 0.5, 0.8, and 1.5×10^{-3} M chloroaurate ions into 0.017 ± 0.001 wt% amyloid fibrils solution (corresponding to Point A, B, and C in **Figure 3**), the planar area of the largest

protein-based filaments organized laterally and twisted into nanofibrils with the diameter of 1–6 nm and the persistent length over 1.0 μm, whose multiple functions as reducing, directing, and stabilizing agents in synthesizing gold platelets have been proposed in our previous research.[8,25,26] β-lactoglobulin for which fibrillization procedure is well-established (e.g., protein 2 wt%, ionic strength <1 × 10⁻³ M, pH 2, 90 °C, and >5 h),[26–28] was selected as a model protein due to its combination of low cost, food grade, and broad availability. As schemed in **Figure 1**A, chloroaurate ions partially bind the surfaces of positively charged amyloid fibrils after mixing homogenously, and are subsequently reduced to elemental gold and forming nuclei. Free available chloroaurate ions continuously diffusing from the solution continue reducing around the nuclei, eventually yielding growing single-crystal gold platelets with final size depending on the delicate balance between nucleation and growth kinetics. After carefully optimizing the
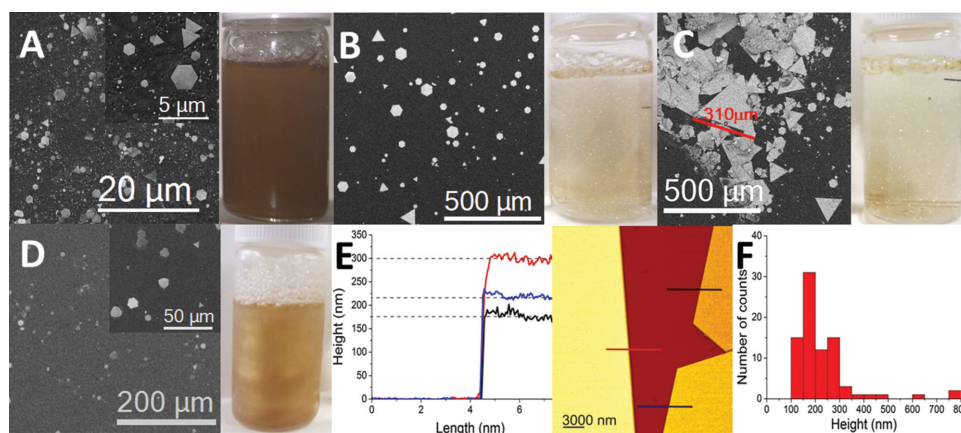

Figure 2. A–D) SEM images (left side) and visual observation (right) of single-crystal 2D gold materials with increasing planar area synthesized with chloroaurate ions and amyloid fibrils of A) 0.5×10^{-3} M, 0.017 wt%; B) 0.8×10^{-3} M, 0.017 wt%; C) 1.5×10^{-3} M, 0.017 wt%; D) 3.2×10^{-3} M, 0.67 wt%. E) Height profiles (left) along the indicated lines in the AFM image (right) of microflakes. F) Thickness histogram plot of single-crystal 2D gold materials.
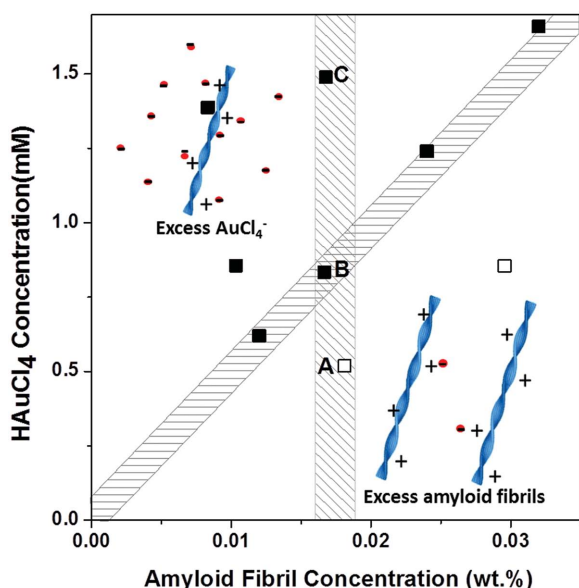
Materials
Views
www.MaterialsViews.com

ADVANCED
MATERIALS
www.advmat.de

COMMUNICATION

Figure 3. Concentration variation of amyloid fibrils and chloroaurate ions for synthesis of single-crystal 2D gold materials at pH ≈ 2 and 60 °C: microflakes (closed symbols) and platelets/nanosheets (open symbols). The insets illustrate two regions separated by a dotted line where there are excess chloroaurate ions or excess amyloid fibrils.

2D gold objects increases 1 to 2 orders of magnitude from 6.5×10^1 (Figure 2A), 3.5×10^3 (Figure 2B) to 8.3×10^4 μm^2 (in Figure 2C). Consistently, the predominant presence of platelets of ≈10^0 μm^2 in Figure 2A yields the characteristic brownish color of the solution. The existence of macroscopic microflakes can be confirmed by visual observations in Figure 2B,C, where mirror-like surfaces of microflakes are distinguishable by naked eyes. Notably, increasing the fibril concentration by over 0.1 wt% is deleterious to microflakes synthesis, e.g., no microflake was observed by varying the concentration ratio between chloroaurate ions and amyloid fibrils (see Figure 2D).[8] This implies that the presence of amyloid fibrils promoting nucleation needs to be maintained low in order to favor growth over nucleation of the crystals.

Atomic force microscopy in Figure 2E further reveals thickness variation of these microflakes, measured by the height profiles along indicated lines. Complete microflakes were not shown due to their large dimensions over thickness. In contrast to ≈25 nm thickness measured for nanosheets (Figure S4, Supporting Information), all these microflakes have thickness above 100 nm, indicating that their unprecedented lateral dimension is occurring together with an average increase in their thickness. The thickness can go as far as ≈800 nm (Figure 2F), eight times larger than the nanosheet thickness of 100 nm ever synthesized through an interface-template method.[17]

The conditions to synthesize single-crystal gold microflakes are summarized in Figure 3, where both the concentrations of chloroaurate ions and amyloid fibrils were varied. It was found that a hypothetical boundary (indicated as the black dotted line), separated two regions for 2D gold nanomaterials: microflakes and nanosheets/platelets. This promptly highlights

the manifold roles of amyloid fibrils for gold synthesis not only as the reducing, directing, and stabilizing agents,[8,25] but also as the nucleation agent. At higher concentrations of amyloid fibrils, chloroaurate ions reduce faster and concentration of nuclei increase, therefore favoring the formation of 2D nanomaterials with smaller size: nanosheets/platelets. On the contrary, higher concentrations of chloroaurate ions favor the growth process of gold, therefore resulting in the formation of 2D nanomaterials with larger size: microflakes.

The increase in size to macroscopic length scale opens up new possibilities for the manufacturing across scales of these materials. For example, microflakes have a stronger tendency to deposit horizontally on substrates when sedimentation occurs naturally in suspensions, compared with gold nanoplatelets,[8] nanocomposites of amyloids and grapheme,[1] and clay-based nanocomposite hydrogels,[29] for which, 2D layer-by-layer orientation is more efficiently achieved by vacuum-filtration methods. Thus, stretchable, conductive composites can be designed by a simple one-step casting approach. For example, the gold microflakes (indicated in Figure 2B) dispersed in a water-dispersion of polyurethane and then casted on polystyrene substrates, leading to free-standing composite films after completely air-drying. As shown in **Figure 4**A, even with less than 10 wt% gold, the film shows homogenous metallic gold color, with smooth and shiny surfaces. Color variation from golden to black, as identified by optical microscopy in Figure 4B, confirms the mirror-like reflecting surfaces of single-crystal microflakes. Further SEM observation of their cross-sections in Figure 4C suggests that gold 2D nanomaterials concentrated and organized layer-by-layer on the bottom sides of the films, as a consequence of their high density (19.32 g cm^{-3} for pure gold in contrast to ≈1.2 g cm^{-3} for polyurethane and 1.0 g cm^{-3} for water). For the sake of comparison, nanosheets (indicated in Figure 2D) were also used to prepare control films (shown in Figure S5A, Supporting Information). In sharp contrast to the insulating composite film containing nanosheets, the film with microflakes is highly conductive on the bottom side (Figure S5B, Supporting Information), within-plane conductivity as high as 4.9×10^3 S cm^{-1}, i.e., two orders of magnitude lower than that of pure gold (4.1×10^5 S cm^{-1}). This indicates that increasing the 2D nanomaterials' size from nanosheets to microflakes leads to sedimentation-driven denser packing, with percolating flakes over the casted film. Moreover, the in-plane conductivity remains constant when bending, twisting or rolling the film (Figure S6, Supporting Information), making the film an ideal candidate for flexible conductors in applications as diverse as flexible displays, field-effect transistors, actuators, electrodes, and smart clothing, etc.

The stretching experiment shows that the films can attain a strain over 500% without failure (Figure S7, Supporting Information). After the strains of 28% (State α), 45% (State β), and 55% (State γ), the stretched films were released and labeled as Sample α, β, and γ, respectively, as shown in Figure 4D. During stretching, Sample α remained highly conductive up to 17.5% and became insulating at a strain of 27% (Figure 4E). This strain-controlling switch effect has been already reported in elastomers' blending or coating with zero/1D metal fillers,[30–34] and with nanosheets coating or patterning flexible films.[9]
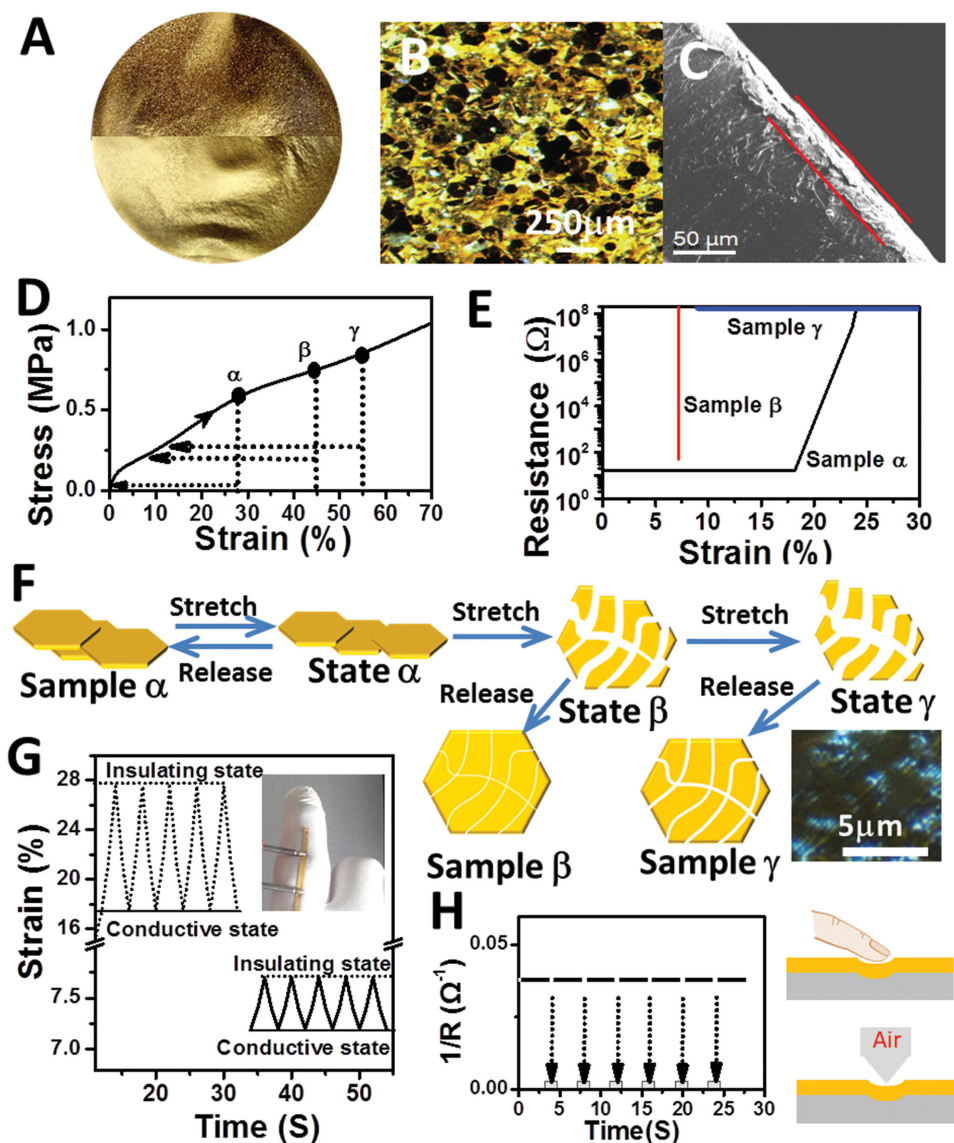
COMMUNICATION

Figure 4. A–C) Front (upper part) and back (bottom part) view of the free-standing polyurethane films (thickness 100 μm) with microflakes as observed by visual observation (A), optical microscopy (B), and SEM cross-section images (C). The gold nanoflake layer is indicated by red lines. D) Stress–strain curve when uniaxially stretching the film. Three strains of 27.5% (α), 45% (β), and 55% (γ) were reached (labeling as State α, β, and γ, respectively) and subsequently released (labeling as Sample α, β. and γ, respectively). E) Strain-dependence of in-plane electric resistance (R) of Samples α, β, and γ (strip size 5 × 10 mm²). F) Schematic representation of microflakes in the film at State α, β, and γ and Sample α, β, and γ. The inset gives an optical microscopy image of a nanoflake in State γ. G) Strain-controlled in-plane conductive and insulating states for Sample α (dotted line) and β (solid line), which can be utilized for sensing finger bending (the inset image). H) Variation of in-plane electric resistance of the film under finger touch (0.037 N) and air force (0.02 N) from a nozzle with the diameter 0.5 mm.

Surprisingly, Sample β has a conductivity switch effect very sensitive to its strain variation, which, to our knowledge, has not been observed before in flexible conductive materials with zero/1D metal fillers. It shifted from metallic conductivity to insulation within a strain variation of 0.5% (Figure 4E). This behavior resulted from breaking the microflakes in the polyurethane matrix when the film is stretched. As shown in Figure 4F, the strain variation first separated the microflakes and then broke the microflakes into pieces (see the inset images in Figures 4F, and S8, Supporting Information). Once the

strain was higher than 55%, the gold pieces were not capable of recovering their initial places; therefore giving a strain-independent insulation state (Sample γ in Figure 4E).

The alteration of in-plane conductive behavior through simply stretching the film to various strains offers an ideal platform for diverse applications, such as strain-sensing devices and electric controllers. For example, from Sample α–β, the increase in strain-sensitivity offers the flexibility of designing an "on–off" switch controlled by different bending degrees in robotics applications (Figure 4G). The high strain-sensitivity of

Materials
Views
www.MaterialsViews.com
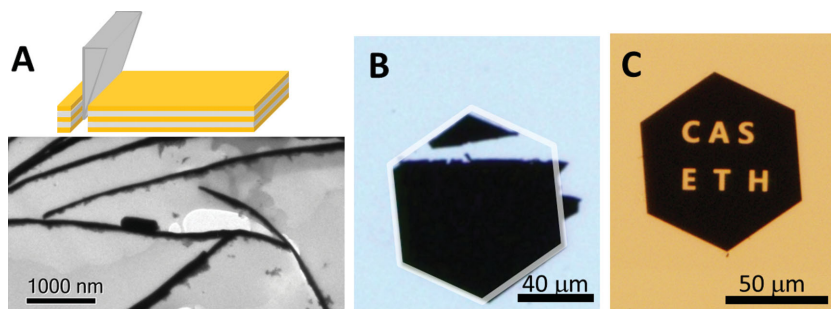
ADVANCED
MATERIALS
www.advmat.de

COMMUNICATION

Figure 5. A) Nanoskiving layer-by-layer organized microflakes for preparation of gold single-crystal nanowires imaged by TEM. B) Removal of one corner from a gold single-crystalline hexagon by mechanical cutting, as imaged by optic microscopy. C) Focused ion beam etching a gold single-crystal microflake with specific letters.

Sample β can further be used to sense force as low as 0.02 N (Figure 4H). For instance, a finger touching the film or an air flux (pressure of 0.1 N mm^{-2}) blowing on it could alter the in-plane electric properties of the film from conductive to insulation states. Similarly, this behavior was also used to sense weak vibration (Figure S9, Supporting Information).

In addition, gold nanomaterials are known for their unique plasmonic resonance features, as well as other promising applications in sensing, imaging, wave guiding, nanoantenna, etc,[6,7] where atomically flat surfaces and single-crystalline features enhance their local plasmonic fields.[7] Owing to their unprecedented planar area, the gold microflakes synthesized in this study may push forward optical nanocircuitry in top-down micro-/nano-fabrication techniques. For example, by nanoskiving layer-by-layer organized microflakes in polymer composites, super long gold nanowire could be prepared (**Figure 5**A). Other shapes can also be obtained by mechanical processing (e.g., cutting in Figure 5B) and focused ion beam etching (Figures 5C and S10, Supporting Information).

In summary, single-crystal gold microflakes with planar area up to and beyond 10^4 µm^2, were fabricated for the first time through a facile, one-step, green approach. By controlling the concentration of β-lactoglobulin amyloid fibrils, acting as reducing, stabilizing, and nucleating agents, over the concentration of chloroaurate ions, a fine tuning in the dimensions of the gold microflakes could be achieved. The unprecedented macroscopic dimensions of these gold single-crystals offer a number of advantages in the applications involving manipulation of 2D microscopic materials. For example, flexible conductive composite films with hierarchical structures, metallic conductivity, and golden optical surfaces were fabricated through simply casting an aqueous polyurethane suspension containing single-crystal gold microflakes, when homologue films based on single-crystal gold nanosheets yielded insulating materials. These films exhibit a unique stain-controlling conductivity behavior, which paves the way to "on–off" switchers and strain/force/vibration sensing devices. This new type of microflakes can ideally serve in optical nanocircuitry, single-crystal electronics, nanoantenna, sensing, and imaging devices in a broad range of micro-/nano-fabrication techniques.

Supporting Information

Supporting Information is available from the Wiley Online Library or from the author.

Acknowledgements

[1] C. Li, J. Adamcik, R. Mezzenga, *Nat. Nanotechnol.* **2012**, *7*, 421.
[2] A. Walther, I. Bjurhager, J.-M. Malho, J. Ruokolainen, L. Berglund, O. Ikkala, *Angew. Chem. Int. Ed.* **2010**, *49*, 6448.
[3] C. Li, A.-K. Born, T. Schweizer, M. Zenobi-Wong, M. Cerruti, R. Mezzenga, *Adv. Mater.* **2014**, *26*, 3207.
[4] C. N. R. Rao, H. S. S. Ramakrishna Matte, U. Maitra, *Angew. Chem. Int. Ed.* **2013**, *52*, 13162.
[5] L. Brus, *Acc. Chem. Res.* **2014**, *47*, 2951.
[6] N. Liu, M. L. Tang, M. Hentschel, H. Giessen, A. P. Alivisatos, *Nat. Mater.* **2011**, *10*, 631.
[7] J.-S. Huang, V. Callegari, P. Geisler, C. Brüning, J. Kern, J. C. Prangsma, X. Wu, T. Feichtner, J. Ziegler, P. Weinmann, M. Kamp, A. Forchel, P. Biagioni, U. Sennhauser, B. Hecht, *Nat. Commun.* **2010**, *1*, 150.
[8] C. Li, S. Bolisetty, R. Mezzenga, *Adv. Mater.* **2013**, *25*, 3694.
[9] G. D. Moon, G.-H. Lim, J. H. Song, M. Shin, T. Yu, B. Lim, U. Jeong, *Adv. Mater.* **2013**, *25*, 2707.
[10] S. Nootchanat, C. Thammacharoen, B. Lohwongwatana, S. Ekgasit, *RSC Adv.* **2013**, *3*, 3707.
[11] C. Bouvy, G. A. Baker, H. Yin, S. Dai, *Cryst. Growth Des.* **2010**, *10*, 1319.
[12] L. Wang, X. Chen, J. Zhan, Y. Chai, C. Yang, L. Xu, W. Zhuang, B. Jing, *J. Phys. Chem. B* **2005**, *109*, 3189.
[13] M. Grzelczak, J. Pérez-Juste, P. Mulvaney, L. M. Liz-Marzán, *Chem. Soc. Rev.* **2008**, *37*, 1783.
[14] X. Huang, X. Qi, Y. Huang, S. Li, C. Xue, C. L. Gan, F. Boey, H. Zhang, *ACS Nano* **2010**, *4*, 6196.
[15] S. S. Shankar, A. Rai, B. Ankamwar, A. Singh, A. Ahmad, M. Sastry, *Nat. Mater.* **2004**, *3*, 482.
[16] J. Jiu, K. Suganuma, M. Nogi, *J. Mater. Sci.* **2011**, *46*, 4964.
[17] H. L. Qin, D. Wang, Z. L. Huang, D. M. Wu, Z. C. Zeng, B. Ren, K. Xu, J. Jin, *J. Am. Chem. Soc.* **2013**, *135*, 12544.
[18] Z. Li, Z. Liu, J. Zhang, B. Han, J. Du, Y. Gao, T. Jiang, *J. Phys. Chem. B* **2005**, *109*, 14445.
[19] D. Wei, W. Qian, Y. Shi, S. Ding, Y. Xia, *Carbohydr. Res.* **2007**, *342*, 2494.
[20] C. A. Goss, D. H. Charych, M. Majda, *Anal. Chem.* **1991**, *63*, 85.
[21] J. Hwang, M. A. Dubson, *J. Appl. Phys.* **1992**, *72*, 1852.
[22] C. Nogues, M. Wanunu, *Surf. Sci.* **2004**, *573*, L383.

[23] K. Banu, T. Shimura, *New J. Chem.* **2012**, *36*, 2112.

[24] T. Kida, *Langmuir* **2008**, *24*, 7648.

[25] S. Bolisetty, J. J. Vallooran, J. Adamcik, S. Handschin, F. Gramm, R. Mezzenga, *J. Colloid Interface Sci.* **2011**, *361*, 90.

[26] J. Adamcik, J.-M. Jung, J. Flakowski, P. De Los Rios, G. Dietler, R. Mezzenga, *Nat. Nanotechnol.* **2010**, *5*, 423.

[27] J.-M. Jung, G. Savin, M. Pouzot, C. Schmitt, R. Mezzenga, *Biomacromolecules* **2008**, *9*, 2477.

[28] J.-M. Jung, R. Mezzenga, *Langmuir* **2010**, *26*, 504.

[29] J. Wang, L. Lin, Q. Cheng, L. Jiang, *Angew. Chem. Int. Ed.* **2012**, *51*, 4676.

[30] D. C. Hyun, M. Park, C. Park, B. Kim, Y. Xia, J. H. Hur, J. M. Kim, J. J. Park, U. Jeong, *Adv. Mater.* **2011**, *23*, 2946.

[31] P. Lee, J. Lee, H. Lee, J. Yeo, S. Hong, K. H. Nam, D. Lee, S. S. Lee, S. H. Ko, *Adv. Mater.* **2012**, *24*, 3326.

[32] M. Park, J. Im, M. Shin, Y. Min, J. Park, H. Cho, S. Park, M.-B. Shim, S. Jeon, D.-Y. Chung, J. Bae, J. Park, U. Jeong, K. Kim, *Nat. Nanotechnol.* **2012**, *7*, 803.

[33] H. Wu, L. Hu, M. W. Rowell, D. Kong, J. J. Cha, J. R. McDonough, J. Zhu, Y. Yang, M. D. McGehee, Y. Cui, *Nano Lett.* **2010**, *10*, 4242.

[34] Y. Kim, J. Zhu, B. Yeom, M. Di Prima, X. Su, J.-G. Kim, S. J. Yoo, C. Uher, N. A. Kotov, *Nature* **2013**, *500*, 59.